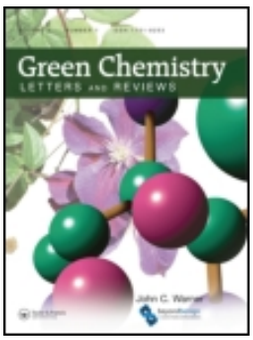

Green Chemistry Letters and Reviews

ISSN: 1751-8253 (Print) 1751-7192 (Online) Journal homepage: http://www.tandfonline.com/loi/tgcl20

Green synthesis of Co_3O_4 nanoparticles via *Aspalathus linearis*: Physical properties

A. Diallo, A.C. Beye, T.B. Doyle, E. Park & M. Maaza

To cite this article: A. Diallo, A.C. Beye, T.B. Doyle, E. Park & M. Maaza (2015) Green synthesis of Co_3O_4 nanoparticles via *Aspalathus linearis*: Physical properties, Green Chemistry Letters and Reviews, 8:3-4, 30-36, DOI: 10.1080/17518253.2015.1082646

To link to this article: https://doi.org/10.1080/17518253.2015.1082646

Published online: 22 Oct 2015.

GREEN CHEMISTRY LETTERS AND REVIEWS, 2015
VOL. 8, NOS. 3-4, 30–36
http://dx.doi.org/10.1080/17518253.2015.1082646

Taylor & Francis
Taylor & Francis Group

LETTER

OPEN ACCESS

Green synthesis of Co_3O_4 nanoparticles via *Aspalathus linearis*: Physical properties

A. Diallo[a,b], A.C. Beye[a,b], T.B. Doyle[a,b], E. Park[a,c] and M. Maaza[a,b]

[a]UNESCO-UNISA Africa Chair in Nanoscienfces-Nanotechnology, College of Graduate Studies, University of South Africa, Muckleneuk ridge, PO Box 392, Pretoria, South Africa; [b]Nanosciences African Network (NANOAFNET), iThemba LABS-National Research Foundation, 1 Old Faure road, Somerset West 7129, PO Box 722, Somerset West, South Africa; [c]Nelson Mandela African Institute of Science & Technology, PO Box 447, Arusha, Tanzania

ABSTRACT

This study reports on the bio-synthesis and the main physical properties of p-type Co_3O_4 nanoparticles for the first time by a completely green chemistry process using *Aspalathus linearis*'s natural extract as an effective chelating agent. Their surface/interface and optical properties are reported. In addition to the X-ray diffraction investigations, the Raman, and infrared as well as X-ray photoelectron spectroscopies confirmed the single phase of the Co_3O_4 nanoparticles. As their average size can be as low as $\langle\phi$particle$\rangle$ ~3.6 nm, the reticular atomic plans are under a slight compressive state.

ARTICLE HISTORY
Received 20 May 2015
Revised 1 August 2015
Accepted 3 August 2015

KEYWORDS
Green chemistry; biosynthesis; cobalt oxide; nanoparticles; *Aspalathus linearis* extract

1. Introduction

Cobalt exhibits several possible oxidation states (Co^{2+}, Co^{3+}, and Co^{4+}), including several types of coordinations (tetrahedral, pyramidal, and octahedral). Consequently, cobalt oxides present a broad field for the creation of many frameworks in view of their stoichiometric and non-stoichiometric oxides, and mixed electronic valency of cobalt, and/or the presence of oxygen vacancies. This multi-electronic valence and rich coordination is proper to cobalt oxides in comparison to other 3d metal oxides. This provides cobalt the ability to be present in various spin states in its oxide forms: low, high, as well as intermediate spin. These probable spin states make the physics of the cobalt oxides attractive from a fundamental viewpoint and in spintronic applications. Such a complexity in spin state originates from the fact that the crystal field splitting of the 3d energy level of the cobalt ion in cobalt oxides is of the same order of magnitude as the Hund's rule intra-atomic exchange energy and the 3d-orbital bandwidth.

Being an antiferromagnetic p-type semiconductor, it is a multi-functional material with several practical applications such as heterogeneous catalysis, electrochromic sensors, pigments and dyes, energy storage, and anode materials in Li-ion rechargeable batteries (*1–6*). Several physical and chemical methodologies to synthesize nanocrystalline Co_3O_4 were used: thermal decomposition of cobalt oxalate, hydrothermal reaction, thermal decomposition of sol-gel derived oxalates, solution combustion method, microwave process, combustion route, among others (*7–13*). Hitherto, yet these physical/chemical methods are very effective, they are complex, and environmentally not generally friendly in view of the required energy balance and/or generated waste. To the best of our knowledge, bio-synthesis of nanoscaled Co_3O_4 was never reported so far. However, it was demonstrated that such an attractive green-approach is successful in the synthesis of metallic nanoparticles as well as some limited oxides (*14–19*).

In this study, we report for the first time, the use of the *Aspallathus linearis*'s natural extract as an effective chelating agent for the facile and rapid bio-synthesis of pure Co_3O_4 single-phase nanoparticles at a low temperature. The fact that there was no use of inorganic/organic solvents neither surfactants nor high temperature makes this synthesis an effective green and eco-friendly process.

2. *Materials and methods*

2.1. *Preparation of the plant extract*

A. linearis of the family Fabaceae, also known as Rooibos, is a plant originally found in the Southern Africa. As shown in Figure 1, *A. linearis* extract contains, among others, two unique phenolic compounds, namely aspalathin (a dihydrochalcone C-glucoside), and aspalalinin (a cyclic dihydrochalcone). Other major phenolic compounds present include flavones (orientin, isoorientin,

CONTACT M. Maaza maaza@tlabs.ac.za

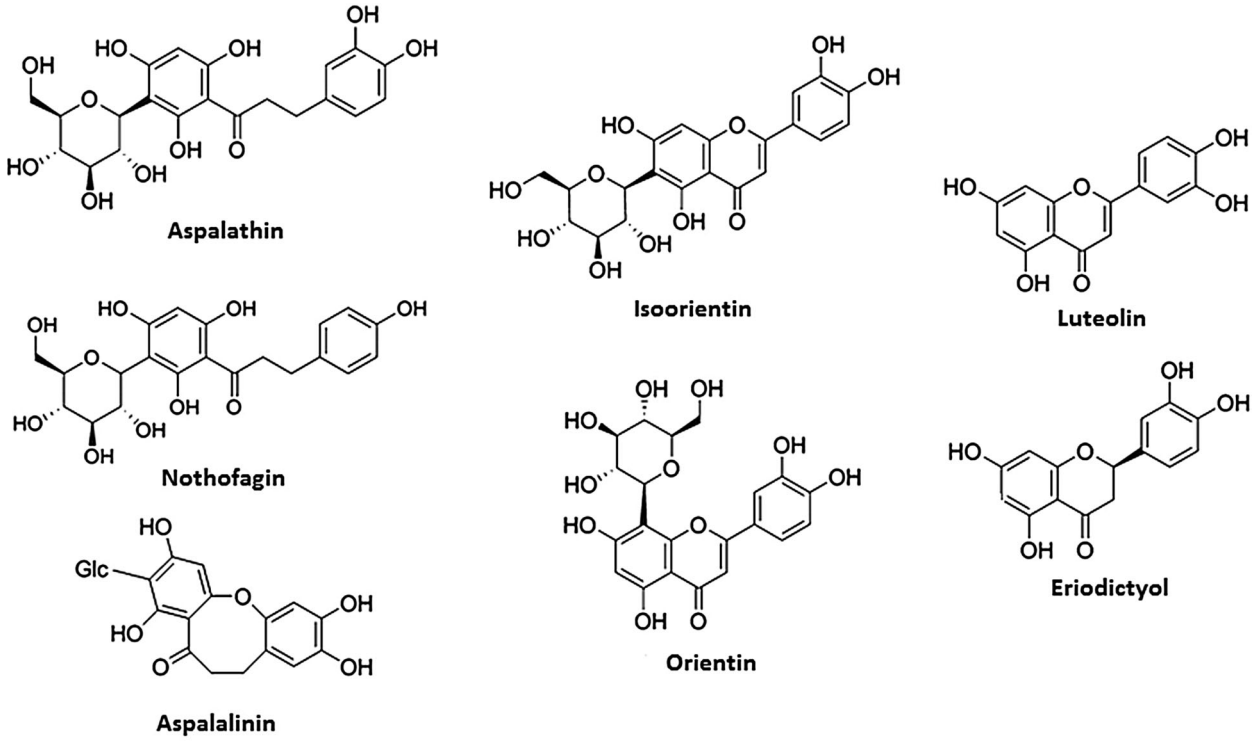

Figure 1. Structure of the various bioactive molecular compounds within the *A. Linearis*'s natural extract.

vitexin, isovitexin, luteolin, chrysoeriol), flavanones (dihydro-orientin, dihydro-isoorientin, hemiphlorin), and flavonols (quercetin, hyperoside, isoquercitrin, rutin) (*20*, *21*). It is established that Aspalathin, which is a rare C–C dihydrochalcone glycoside, and the two structurally related chalcones (nothofagin and aspalalinin) are the most bioactive compounds. These bioactive components are believed to be potential chemical reduction agents (*20*, *21*).

High-quality dried *A. linearis* leaf powder was weighted and cleaned extensively with deionized cold H_2O (15°C). Following a drying phase under sunny conditions at ambient temperature (26°C), the samples were ground. An estimated 8 g of *A. Linearis* leaf powder was mixed with 300 ml of de-ionized H_2O at 25°C for 48 h. The duration of 48 h was considered to ensure the maximum extraction of the bioactive compounds (highlighted in Figure 1) from the ground *A. Linearis* leaf powder. This was verified by UV–VIS–NIR spectroscopy; the optical absorbance spectrum does not change for higher extraction periods. The brown solution was filtered two times to eliminate residual solids (if any). The extracted natural dye has a pH of 5 at room temperature. The homogeneous mixture with the Cobalt precusor dropped to a pH of 3.8. One has to mention that the used *A. Linearis* leaf extract is slightly fermented so as to minimize and even preclude the oxidation of the green leaves' polyphenols. The chemical composition is nearly similar to that of fresh leaves except for few enzymatically catalyzed changes which occur with extreme rapidity following plucking, as in the case of green tea (*22*).

2.2. *Synthesis of the Cobalt oxide nanoparticles and characterization*

A. linearis's natural extract was used to reduce several Cobalt-based salts, including Cobalt nitrate hexahydrate ($Co(NO_3)_2$ $6H_2O$, melts 55°), Co Chloride hexahydrate ($CoCl_2$ $6H_2O$, d 87), and Co hydroxide ($Co(OH)_2$ D. 160) as well as Ammonium-Cobalt (II)-sulfate-hexahydrate ($(NH_4)_2Co(SO_4)_2{\cdot}6H_2O$))-based precursors. This communication focuses on the green reduction of Co $(NO_3)_2{\cdot}6H_2O$ initial precursor as a proof of concept of bio-synthesis of single-phase Co_3O_4 nanoparticles. Analytical grade reagent Co $(NO_3)_2{\cdot}6H_2O$ from Sigma-Aldrich was used. Dry leaves of *A. linearis* from its original region (i.e. the Cederberg region, South Africa) were used. In a typical set-up, 6.65 g of the *A. linearis* leaves were heated in 250 ml of de-ionized water at a temperature between 75°C and 85°C for 2–3 h, yielding a brown extract (pH = 5). To the filtered brown aqueous extract obtained after cooling to room temperature was added to a 6.0 g of $Co(NO_3)_3{\cdot}6H_2O$ solution of pH of 3.8. At room temperature, while swirling, the Co salt was observed to dissolve completely in the aqueous extract under 3 mins. The resultant solution was allowed to settle over a period of 24 h, after which a precipitate was observed without

any heating. The precipitate was then separated from the aqueous extract, first by decanting then by centrifuging at 1000 rpm 3 times for 10 min each over successive additions of de-ionized water to wash the precipitate of any residual aqueous extract. As the synthetized oxides-based nanoparticles by green process are generally amorphous, an annealing was necessary to induce an effective crystallization (*23–32*). In this case, the as-obtained centrifuged precipitate was heated at 90°C for 90 min to remove bio-compounds in excess. Following such a phase, the Co-based precipitate was submitted to annealing during 2 h in air at several temperatures: 100°C, 300°C, 400°C, and 500°C.

Various characterizations were carried out on the annealed powder. For the High Resolution Transmission Electron Microscopy (HRTEM), a Jeol JEM 4000EX electron microscopy unit with a resolution limit of about 0.12 nm, equipped with a Gatan digital camera, was used. The Energy Dispersive X-Ray Spectroscopy (EDS) spectrum was collected with an Oxford instruments X-Max solid-state Silicon drift detector operating at 20 keV. The crystallographic properties were recorded by using X-ray Diffraction (XRD) Model Bruker AXS D8 Advance of radiation Cu(Kα . 1.5406 Å) and a Jobin-Yvon-SPEX integrated Raman spectroscopy. The FT–IR spectra of (as pellets in KBr) were recorded in ABB Bomem MB series instrument. For the X-ray Photoelectron Spectroscopy (XPS), a VG Scientific LAB MK-II spectrometer with an Mg–Ka X-ray source (1253.6 eV) was used. The pressure inside the chamber was held below 5–10^{-8} Torr during analysis. The carbon C(1s) electron binding energy corresponding to graphitic carbon was referenced at 284.6 eV for calibration of Co(2p) and O(1s) core level peaks.

3. Results and discussion

3.1. *Morphology and size distribution*

Figure 2 shows the typical observations made using transmission electron microscopy (TEM), (Figure 2(a)) and HRTEM (Figure 2(c)) observations on the precipitate annealed at 100°C. More accurately, Figure 2(a) shows that the synthesized powder consists of non-agglomerated quasi-spherical in shape nanoparticles. Following a digitization phase of various images such as Figure 2(a), the average diameter of the particles ranging from 2 to 7 nm estimated by fitting the histogram data with a Log-Normal distribution was $\langle \phi_{particle} \rangle \sim 3.57$ nm with a 0.05 nm of standard error (Figure 2 (b)). To conclude on the degree of crystallinity of the nanoparticles, several HRTEM observations (Figure 2 (c)) and Selective Area Electron Diffraction analysis were carried out (Figure 2(d)). From such observations, it was noticed that, statistically, the bulk of the nanoparticles exhibited a low-range atomic ordering

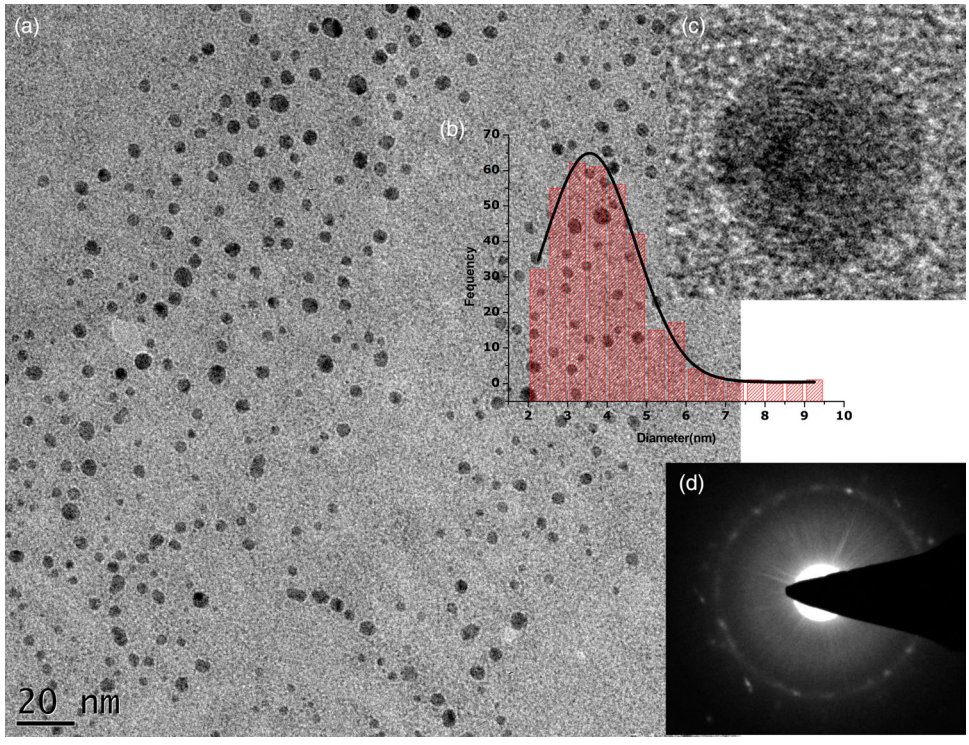

Figure 2. TEM images (at various magnifications) of the cobalt oxide nanoparticles, with their size distribution and a typical electron diffraction pattern.

(Figure 2(b) and 2 (d)). The major of the nanoparticles were amorphous.

3.2. *Elemental composition*

Figure 3 shows a typical EDS spectrum on the annealed sample at 100°C. Excluding the Carbon from the Carbon-coated Copper grid, no other elements are observed except Cobalt and Oxygen. Hence, one could conclude that the chemical reduction of the hexahydrated $Co(NO_3)_2{\cdot}6H_2O$ precursor is complete, which is in line with the XRD results presented in Section 3.3. The average Co/O atomic ratio deduced from the EDS studies is about 2.91/3.95, which is, within the bar error, consistent with the theoretical value of ¾, that is, Co_3O_4 and not CoO neither Co_2O_3 nor Co hydroxide $Co(OH)_2$. No other element has been detected so far, indicating, a priori, the significant chemical purity of the Co_3O_4 nanoparticles following the preparation and final filtration protocol.

3.3. *Crystallography and atomic structure*

Figure 4 reports the room temperature XRD pattern of the annealed filtered precipitate. All observed Bragg peaks are indexed in line with the JCPDS card 00-042-1467 of the face-centered cubic Co_3O_4 with an average lattice parameter $\langle a_{exp}\rangle$= 8.071 Å ($\langle a_{bulk}\rangle$= 8.08370 Å) highlighting the purity of synthetized Co_3O_4 crystallites and the absence of any crystallographic texture. As the lattice difference $(\langle a_{exp}\rangle\text{-}\langle a_{bulk}\rangle)/\langle a_{bulk}\rangle$ is ∼ –0.16%, one could deduce that the reticular plans are slightly compressed. The Bragg peaks are broad with a width at half maximum $\langle \Delta\Theta_{1/2}\rangle$ ∼1 deg sustaining the nano-

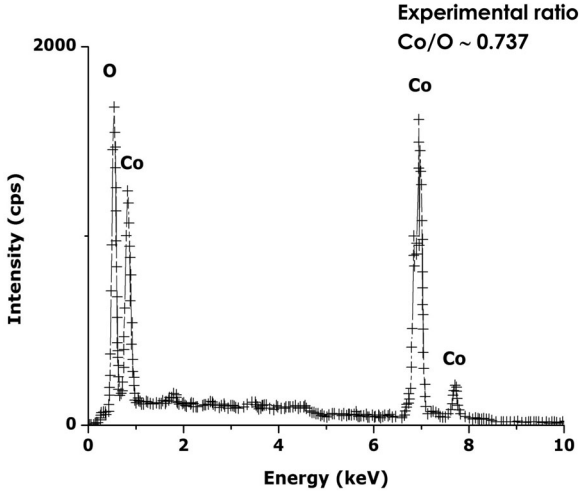

Figure 3. Typical electron dispersion spectrometry profile of the annealed cobalt oxide nanoparticles.

scaling of the synthesized Co_3O_4 crystallites even after the heat treatment of ∼400°C.

3.4. *Vibrational properties*

To sustain the purity of the synthesized Co_3O_4 nanoparticles, room temperature Raman spectroscopy studies were carried out. As highlighted previously, the Co_3O_4 with Co^{2+} ($3d^7$) and Co^{3+} ($3d^6$) located at tetrahedral and octahedral sites, respectively, crystallizes in a spinel configuration for which the space group theory predicts the following active modes as an "Fd3m" symmetry: $\Gamma = A_{1g}$ (R) + E_g (R) + F_{1g} (IN) + $3F_{2g}$ (R) + $2A_{2u}$ (IN) + $2E_u$ (IN) + $4F_{1u}$ (IR) + $2F_{2u}$ (IN), where (R), (IR), and (IN) represent Raman active vibrations, infrared-active vibrations, and inactive modes, respectively. Figure 5 shows the typical Raman spectrum of the annealed Cobalt oxide nanoparticles. One can distinguish six active Raman modes; they are approximately located at ∼185.5, ∼465.3, ∼506.6, ∼601, ∼670, and ∼755.5 cm^{-1}. Excluding the last mode, all observed modes are in agreement with the values of pure Co_3O_4 spinel structure yet with an average shift of the order of $\Delta v \sim 5\ cm^{-1}$ (191, 470, 510, 608, and 675 cm^{-1}). While the Raman mode at 684.5 cm^{-1} is attributed to characteristics of the octahedral sites A_{1g}, the E_g, and F_{2g} modes are related to the combined vibrations of tetrahedral site and octahedral oxygen motions (*23*). The average shift of $\Delta v \sim 5\ cm^{-1}$ may be attributed to size effects or surface stress/strain.

To validate once more the spinel Co_3O_4 nature of the synthesized particles and their purity, Attenuated Total Reflection-Fourier Transform Infrared spectroscopy (ATR-FTIR) studies were conducted at room temperature. Figure 6 reports the typical ATR-FTIR spectrum of the annealed Cobalt oxide nanoparticles in the spectral range of 400–4000 cm^{-1}. The IR optical transmission is plotted versus the Log of the wavenumber so as to single out the major IR absorptions observed at lower wavenumbers. Two main relatively sharp absorptions centered at ∼570 and ∼668 cm^{-1}. These modes correspond to the so-called absorption bands v_1 (at 565 cm^{-1}) and v_2 (661 cm^{-1}), which originate from the fingerprint stretching vibrations of the Cobalt-Oxygen bond of the Co_3O_4 spinel oxide (*24*). More precisely, the observed 570 cm^{-1} band is characteristic of O–Co with Co denoting the Co^{3+} in the octahedral site) while the 668 cm^{-1} band is attributable to the Co^{2+} $Co^{3+}O_3$ (the Co^{2+} being in the tetrahedral site) vibration in the spinel lattice (*25*, *26*). In addition, the ATR-FTIR spectrum shows no residual organic compounds such as NO_3^- after filtration and centrifugation. A weak and wide

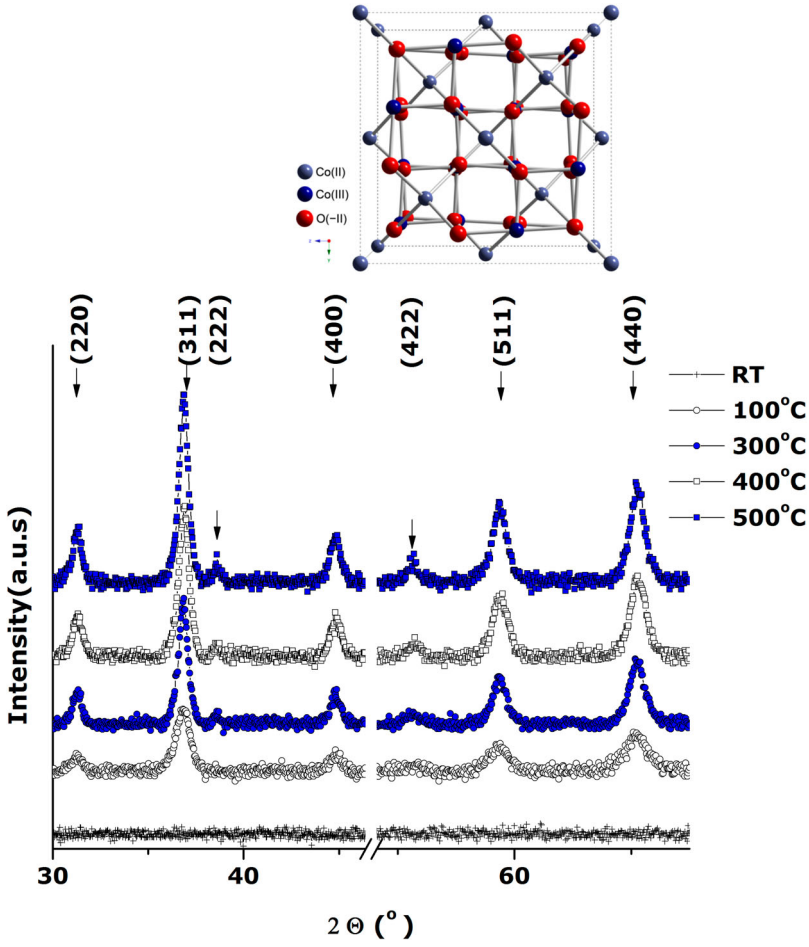

Figure 4. Typical room temperature X-ray diffraction of the annealed Co_3O_4 nanoparticles.

asymmetric band centered at about 1627 cm^{-1} could be attributed to the presence of OH^- groups due to the absorption of atmospheric water vapor by the nanoparticles.

3.5 *Surface-interface properties*

To support the previous EDS, XRD, Raman, and the ATR-FTIR results, XPS investigations were carried out. The XPS investigations were conducted using a constant 50 eV pass energy mode, in 0.1 eV increments at a 50 ms

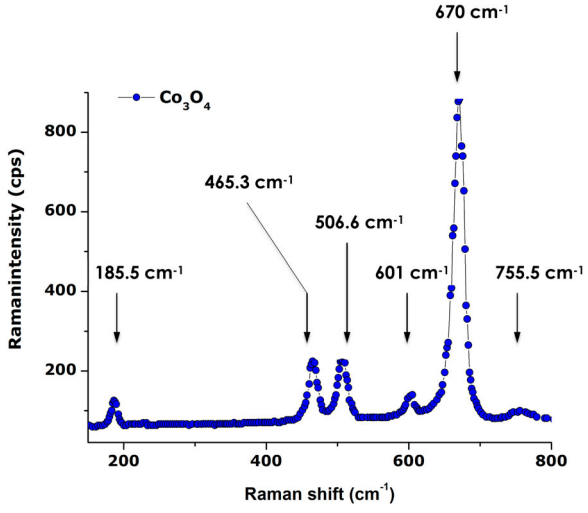

Figure 5. Typical Raman spectrum of the annealed Co_3O_4 nanoparticles.

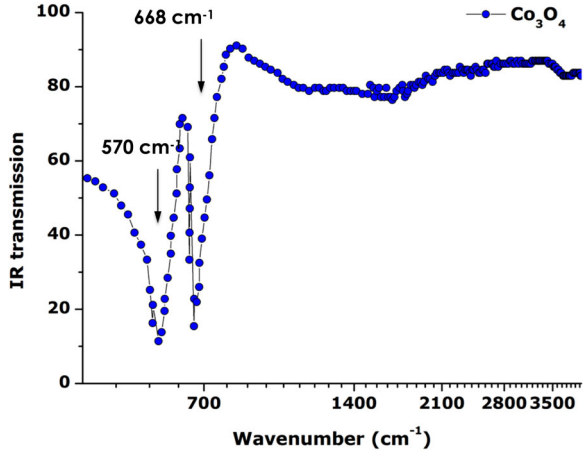

Figure 6. Typical Attenuated Total Reflection FTIR spectrum of the annealed Co_3O_4 nanoparticles.

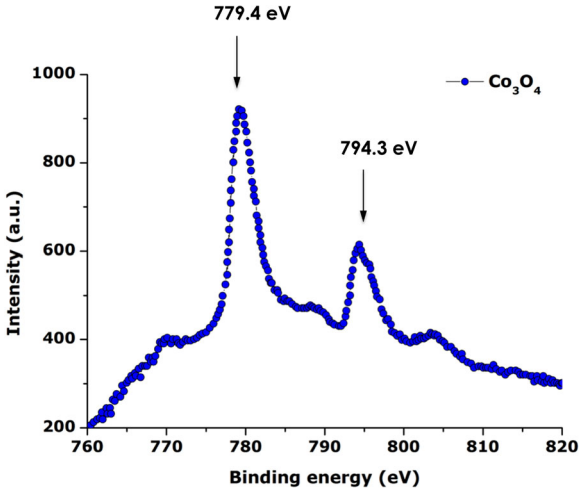

Figure 7. Typical Co_{2p} X-ray photoemission spectroscopy spectrum of the annealed Co_3O_4 nanoparticles.

dwell time with the signal averaged for at several regular scans. Figure 7 shows the typical XPS spectrum of the annealed Cobalt oxide nanoparticles. More precisely, it reports the characteristic Co_{2p} peaks and corresponding binding energies. The $2p_{1/2}$ and $2p_{3v/2}$ are centered at 779.4 and 794.3 eV. The Co_{2p} and O_{1s} regions are consistent with stoichiometric Co_3O_4 (*27*).

3.6. *Pre-conclusion*

While the TEM, HRTEM, and XRD investigations demonstrated the nano-scale aspect of the synthesized particles, the XRD, EDS, ATR-FTIR, Raman, and XPS spectroscopy combined studies sustained the nature and/or single phase of the Co_3O_4 nanoparticles. Yet this green methodology has been validated for several other nano-oxides such as CdO, ZnO, In_2O_3, Mn_3O_4, and Cr_2O_3 using *A. Linearis* leaf extract (*28*–*32*); the mechanism of formation of such nanoparticles is not understood and is being investigated using *in situ* and *ex situ* High Performance Liquid Chromatography and Liquid Chromatography Mass Spectrometry. As mentioned previously, *A. Linearis* leaf extract contains, among others, two unique phenolic compounds: aspalathin (a dihydrochalcone C-glucoside) and aspalalinin (a cyclic dihydrochalcone). Other major phenolic compounds present include flavones, flavanones, and flavonols (*21*, *22*). It is established that the phenolic compounds exhibit higher antioxidant potential and therefore possess a significant reduction capacity of metal ions, hence favoring the green synthesis of nanoparticles. In addition, the high content of proteins, lipids as well as amino acids contribute to stabilize the growth of such nanoparticles while inhibiting their agglomeration (*20*).

4. Conclusions

The green synthesis of high-purity amorphous Co_3O_4 quasi-spherical nanoparticles ($\langle\phi_{particle}\rangle$ ~3.57 nm) by green process using the natural extract of *A. Linearis* as an effective bio-reduction/bio-oxidizing chemical agent was demonstrated. Thermal annealing at ~400°C during 2 h under normal air conditions allows the acquisition of crystallized single-phase Co_3O_4 nanoparticles as substantiated by the EDS, XRD, Raman, ATR-FTIR, and XPS investigations. The follow-up study will consist of identifying the mechanism (s) and will follow the dynamic of formation of the Co_3O_4 nanoparticles during the interaction of the Co precursor and the *A. Linearis* extract.

Disclosure statement

No potential conflict of interest was reported by the authors.

Funding

This research program was generously supported by grants from the National Research Foundation of South Africa (NRF); Centre National pour la Recherche Scientifique, France; iThemba LABS; the UNESCO-UNISA Africa Chair in Nanosciences & Nanotechnology; the Organization of Women in Science for the Developing World (OWSDW); and the Abdus Salam ICTP via the Nanosciences African Network (NANOAFNET) as well as the African Laser Centre (ALC).

References

(1) Askarinejada, A.; Bagherzadehb, M.; Morsali, A. *Appl. Surf. Sci.* **2010,** *256,* 6678–6682.
(2) Li, W.; Xu, L. J. *Chen, Adv. Funct. Mater.* **2005,** *15,* 851–857.
(3) Shinde, V.R.; Mahadik, S.B.; Gujar, T.P.; Lokhande, C.D. *Appl. Surf. Sci.* **2006,** *252,* 7487–7492.
(4) Kaviyarasu, K.; Raja, A.; Anand Devarajan, P. *Spectrochim. Acta. A. Mol. Biomol. Spectrosc.* **2013,** *114,* 586–591.
(5) Jodłowski, P.J.; Jędrzejczyk, R.J.; Rogulska, A.; Wach, A.; Kuśtrowski, P.; Sitarz, M.; Łojewski, T.; Kołodziej, A.; Łojewska, J. *Spectrochim. Acta. A. Mol. Biomol, Spectrosc.* **2014**, 131, 696–701.
(6) Li, X.; Zhang, Z.; Tao, L.; Gao, M. *Spectrochim. Acta. Part A. Mol. Biomol. Spectrosc.* **2013,** *107,* 311–316.
(7) Salavati-Niasari, M.; Mir, N.; Davar, F.J. *J. Phys. Chem. Solids.* **2009,** *70,* 847–852.
(8) Dong, C.; Xiao, X.; Chen, G.; Guan, H.; Wang, Y. *Mater. Lett.* **2014,** *123,* 187–190.
(9) Thota, S.; Kumar, A.; Kumar, J. *Mater. Sci. Eng. B.* **2009,** *164,* 30–37.
(10) Makhlouf, M.Th.; Abu-Zied, B.M.; Mansour, T.H. *Appl. Surf. Sci.* **2013,** *274,* 45–52.
(11) Zhang, P.; Hu, G.; Bao, S.; Guo, J.; Lei, C.; Cai, C.; Jia, D.Z.; Wang, R. *Mater. Lett.* **2012,** *83,* 195–197.

(12) Dai, G.; Liua, S.; Lianga, Y.; Luo, T. *Appl. Surf. Sci*. **2013,** *264,* 157–161.
(13) Li, H.; Fei, G.T.; Fanga, M.; Cui, P.; Guoa, X.; Yana, P.; Zhanga, L.D. *Appl. Surf. Sci*. **2011,** *257,* 6527–6530.
(14) Mahdi Pourmortazavi, S.; Taghdiri, M.; Makari, V.; Rahimi-Nasrabadi, M. *Spectrochim. Acta Part A. Mol. Biomol. Spectrosc*. **2015,** *136,* Part C, 5, 1249–1254.
(15) Sinha, T.; Ahmaruzzaman, M. *Spectrochim. Acta Part A. Mol. Biomol. Spectrosc*. **2015,** *145,* 280–288.
(16) Malleshappa, J.; Nagabhushana, H.; Kavyashree, D.; Prashantha, S.C.; Sharma, S.C.; Premkumar, H.B.; Shivakumara, C. *Spectrochim. Acta Part A. Mol. Biomol. Spectrosc*. **2015,** *145,* 63–75.
(17) Elumalai, K.; Velmurugan, S.; Ravi, S.; Kathiravan, V.; Ashokkumar, S. *Spectrochim. Acta Part A. Mol Biomol Spectrosc*. **2015,** *143,* 158–164.
(18) Kaviyarasu, K.; Raja, A.; Devarajan, Prem Anand. *Spectrochim. Acta. Part A. Mol. Biomol. Spectrosc*. **2013,** *114,* 586–591.
(19) Sivakumar, S.; Venkatesan, A.; Soundhirarajan, P.; Prasad Khatiwada, C. *Spectrochim. Acta Part A. Mol. Biomol. Spectrosc*. **2015,** *136,* 1751–1759.
(20) Joubert, E.; de Beer, D. *S. Afr. J. Bot*. **2011,** *77,* 869–886.
(21) Aragonès, M.; Camps, G.; Alonso-Villaverde, J.; Menéndez, C.; Micol, J.A.; Segura-Carretero, V.; Joven, A. *J. Phytomedicine*. **2011,** *18,* 414–424.
(22) Senthilkumar, S.R.; Sivakumar, T. *Int J. Pharm. Pharm. Sci*. **2014,** *6* (6), 462–465.
(23) Abu-Zied, B.M.; Soliman, S.A. *Catal. Lett*. **2009,** *132,* 299–310.
(24) Ren, L.; Wang, P.; Han, Y.; Hu, C.; Wei, B. *Chem. Phys. Lett*. **2009,** *476,* 78–83.
(25) Ai, L.-H.; Jiang, J. *Powder Technol*. **2009,** *195,* 11–14.
(26) Salavati-Niasari, M.; Mir, N.; Davar, F. *J. Phys. Chem. Solids*. **2009,** *70,* 847–852.
(27) Petitto, S.C.; Marsh, E.M.; Carson, Gr.A.; Langell, M.A. *J. Molecul. Catal. A: Chem*. **2008,** *281,* 49–58.
(28) Thema, F.T.; Beukes, P.; Gurib-Fakim, A.; Maaza, M. *J. Alloys Comp*. **2015**, 646, 1043–1048.
(29) Diallo, A.; Ngom, B.D.; Park, E.; Maaza, M. *J. Alloys Comp*. **2015**, 646, 425–430.
(30) Thema, F. T.; Manikandan, E.; Dhlamin, M.S.; Maaza, M. *Materials Letters*, **2015**. doi:10.1016/j.matlet.2015.08.052.
(31) Thovhogi, N.; Diallo, A.; Gurib-Fakim, A.; Maaza, M. *J. Alloys Comp*. **2015**, 647, 392–396.
(32) Sone, B.T.; Manikandan, E.; Gurib-Fakim, A.; Maaza, M. *J. Alloys Comp*. **2015**, 650, 357–362.